Research Square

Preprints are preliminary reports that have not undergone peer review.
They should not be considered conclusive, used to inform clinical practice,
or referenced by the media as validated information.

Reinforcement of paper sheets with subcritical water-treated cellulose for improved mechanical strength and barrier properties

Suhyeon Nam
Ewha Womans University
Jiho Lim
Ewha Womans University
Soohyun Kim
Ewha Womans University
Ji Hun Park
Ewha Womans University
Hansol Doh
hdoh@ewha.ac.kr
Ewha Womans University

Research Article

Keywords: Paper-based packaging, subcritical water-treated cellulose, mechanical reinforcement, barrier properties

Posted Date: May 19th, 2026

DOI: https://doi.org/10.21203/rs.3.rs-8586248/v1

License: This work is licensed under a Creative Commons Attribution 4.0 International License.
Read Full License

Additional Declarations: No competing interests reported.

Abstract

The excessive use of non-biodegradable plastics has raised serious environmental concerns, indicating the urgent need for biodegradable packaging materials. Thus, paper packaging systems have gained increasing attention. However, their weak mechanical strength and insufficient barrier properties limit their practical applications. To address these limitations, a paper-based packaging system reinforced with subcritical water-treated cellulose (SWT-C) was developed to enhance mechanical and barrier properties in this study. The specimens were prepared by incorporating varying concentrations of SWT-C into softwood and hardwood pulps. Their structural, physical, and chemical characteristics were evaluated using SEM images, FTIR analysis, XRD test, and BET surface area measurements. Mechanical properties were evaluated with tensile test and barrier performance was assessed by Cobb60 water absorption test and oil and grease resistance (OGR) test. As a result, the pore volume of both pulps decreased from 0.9546 cm^3/g to 0.04253 cm^3/g with increasing SWT-C incorporation, as confirmed by SEM observations and BET analysis. This reduction in porosity may contribute to an increase in tensile strength, reaching a maximum of 35.91 MPa. Both paper sheets reinforced with SWT-C showed a substantial reduction in Cobb60 and OGR tests, indicating enhanced water and oil resistance. In conclusion, SWT-C improved the performance of paper sheets mainly through pore filling, network densification, and hydrogen bonding reinforcement. The findings in this study demonstrate that SWT-C serves as an effective reinforcing agent to improve the mechanical strength and barrier properties of paper packaging system, thereby showing its potential for application in the industry.

Introduction

Instead of plastic packaging systems, which pose significant environmental challenges due to their non-biodegradability and potential to cause pollution, paper packaging systems have increased interest recently to maintain environmental sustainability (Oh et al. 2022). Although the paper packaging system has several advantages, including abundant availability, biodegradability, and recyclability, it faces significant limitations in mechanical and barrier properties. The low tensile strength of paper is primarily due to the weak non-covalent interactions—mainly hydrogen bonds, along with minor contributions from hydrophobic interactions and dispersion forces—between cellulose fibers, which make it vulnerable to tearing and deformation under mechanical stress (Wohlert et al. 2022). In addition, the relatively large pore size of paper packaging system further weakens its barrier properties, allowing external substances such as moisture, oxygen, and oils to penetrate more easily. As a result, cellulosic-based paper packaging system fails to effectively block the permeation of moisture, oxygen, oils, and other external substances that can negatively affect the quality of products, thereby limiting its application as a reliable packaging material (Alava and Niskanen 2006). To solve these problems, paper packaging systems usually select surface coating strategies to improve their mechanical, barrier, and thermal properties with conventional plastics such as polyethylene (PE) and polylactic acid (PLA) (Furuheim et al. 2004; Marzbani et al. 2021; Lei et al. 2024). However, in terms of environmental pollution, the effects of plastic coating systems on paper packaging offer no advantages.

To address these limitations, the addition of nanocellulose in the pulp matrix for paper packaging material has gained increased interest (Lu et al. 2023; Li et al. 2021; Perdoch et al. 2022). Nanocellulose plays a key role as a reinforcement agent in the polymer matrix and it is well-known for improving mechanical, barrier, and thermal properties (Perdoch et al. 2022; Abdul Rashid et al. 2018). Although many other agents are used for enhancing the mechanical and barrier properties of paper packaging materials, nanocellulose is known as one of the most effective reinforcement agents because of its high aspect ratio and large surface area, which contribute to improvements in mechanical, barrier, and thermal properties (Deng et al. 2017). In addition, since both paper packaging materials and nanocellulose are composed of cellulose, they exhibit strong molecular compatibility through hydrogen bonding, thereby enhancing the reinforcement efficiency without the need for additional treatments such as plasma discharge, corona treatment, primer coating, or impregnation (Hubbe et al. 2008; Laleicke and Hubbe 2025). For instance, Lu et al. (2023) reported that incorporating cellulose nanofiber (CNF) into paper sheets at 50% wet solids content increased the tensile strength in the machine direction up to 4.49 N·m/g with the help of the formation of numerous hydrogen bonds between nanocellulose and polymer matrix. Furthermore, Guan et al. (2019) investigated the effect of incorporating CNF into bamboo pulp-based tissue paper and found that the tensile strength significantly increased from 18.5 to 24.5 Nm/g with the addition of 10 wt% CNF.

Despite the advantages of incorporating nanocellulose into paper packaging system, current extraction process of nanocellulose raises significant environmental concerns. The extraction process for CNF typically involves the use of 2,2,6,6-Tetramethylpiperidine-1-oxyl (TEMPO) which requires large amounts of water and may contribute to environmental pollution and consumer apprehension (Barbash et al. 2022). Additionally, cellulose nanocrystals (CNCs), which is the other type of nanocellulose using reinforcement agent in packaging system, is commonly extracted though acid hydrolysis using sulfuric acid (H_2SO_4) (Mohomane et al. 2022). Since this extraction process also requires a substantial amount of water to remove residual reagents and neutralize acidic by-products, methods for obtaining nanocellulose lead to significant waste-water generation, which causes environmental burden (Li et al. 2015). Moreover, the yield of these methods for converting micron-scale cellulose into nanocellulose is typically low, ranging from 13.3% to 26.1%, resulting in increased costs for paper packaging. Therefore, the current approaches present challenges due to their complexity and the difficulty of scaling up for large-scale production (Doh et al. 2020). These challenges highlight the urgent need for more sustainable and efficient extraction methods for conventional nanocellulose.

Subcritical water-treated cellulose (SWT-C) is defined as cellulose that is treated by subcritical water. Subcritical water treatment (SWT) utilizes only water under conditions just below its critical point, thereby reducing the need for hazardous chemicals or organic solvents (Prakash et al. 2020; Novo et al. 2015; Rafeny et al. 2023). Under the subcritical conditions at temperatures of 140–200°C and reaction times of 20–60 min, the dielectric constant of water decreases to levels similar to those of organic solvents, which promotes the selective hydrolysis of amorphous regions in cellulose (Kim et al. 2026; Ko et al. 2020; Osei-Bonsu et al. 2024). This approach enables efficient hydrolysis of cellulose bundles while minimizing environmental impact, as it avoids the use of strong chemical agents and generates no toxic

by-products (Ko et al. 2020; Adschiri et al. 1993; Novo et al. 2015; Osei-Bonsu et al. 2024). Therefore, the SWT is considered as an eco-friendly and sustainable alternative to obtain nanocellulose. Our research team successfully prepared SWT-C from microcrystalline cellulose (MCC) with enhanced physicochemical properties compared to conventional nanocellulose and applied it as a reinforcing material in sustainable and eco-friendly paper packaging systems.

Overall, SWT-C reinforced paper sheet was developed as a novel paper-based packaging material in this study. The physicochemical properties of developed paper packaging materials were evaluated with a focus on the mechanical strength and barrier properties against water, oil, and grease of paper sheets as a function of SWT-C contents, changes in chemical structure, and variations in crystallinity. Furthermore, the effects of SWT-C addition were evaluated through surface morphology and pore size analysis to assess structural properties. The novel aspects of this study are: (1) the addition of SWT-C as sustainable reinforcement agent for paper packaging system, (2) the use of two different pulps to evaluate the reinforcing functionality of SWT-C in paper sheets, and (3) the elucidation of the correlation between SWT-C and the mechanical strength and barrier properties of the developed paper packaging system.

Materials and Methods

Materials

8495-Northern Softwood Bleached Kraft Pulp (SW) was purchased from The Procter & Gamble Cellulose Company (Cincinnati, OH, USA), and 8496-Eucalyptus Hardwood Bleached Kraft Pulp (HW) was prepared from Aracruz Celulose S.A. (Aracruz, Espírito Santo, Brazil). MCC was obtained from Carl Roth (Karlsruhe, Land Baden-Württemberg, Germany). Sodium hydroxide (NaOH) was purchased from Daejung Chemicals & Metals Co. (Siheung, Gyeonggi-do, South Korea). Urea ($(NH_2)_2CO$, 99% purity), Castor oil, n-Heptane ($CH_3(CH_2)_5CH_3$, 98% purity), toluene ($C_6H_5CH_3$, 99.5% purity) was obtained from Samchun Chemical Co. (Pyeongtaek-si, Gyeonggi-do, South Korea). Whatman No. 42 filter paper (pore size 2.5 μm, Cytiva, Marlborough, MA, USA) was prepared.

Preparation and characterization of SWT-C

MCC was treated in a SWT equipment (ChemRe SYStem Inc., Anyang-si, Gyeonggi-do, South Korea) at 160°C, 60 bar, for 30 min. Distilled water was used as the solvent at a ratio of 1 g of MCC per 100 mL of distilled water and loaded into the treatment cell. After the treatment, the remaining solid material in the cell, referred to as SWT-C, was collected on a stainless-steel tray and dried at 40°C until the moisture content was below 3%. The dried SWT-C was then ground, sieved to under 50 μm, and stored at room temperature.

The morphology of SWT-C was analyzed using a high-performance transmission electron microscope (TEM; JEM-2100F, JEOL Ltd, Tokyo, Japan), operating at an accelerating voltage of 200 kV. Image J

software (National Institutes of Health, Bethesda, MD, USA) was used for analyzing the length and width of SWT-C.

Crystallinity was determined with an X-ray diffractometer (D8-Advance, Bruker, Karlsruhe, Germany) at a scanning rate of 0.2 sec/step from 5° to 60° using a voltage and current of 40 kV and 40 mA, respectively. The crystallinity index of the sample was calculated by the Segal method (Segal et al. 1959) using the following equation:

$$X_{CR}\,(\%) = \frac{I_{002} - I_{AM}}{I_{002}} \times 100$$

1

where I_{002} represents the maximum intensity at 20–22° peak, and I_{AM} represents the minimum intensity at 17–20° region.

The FTIR spectra of SWT-C were examined in the infrared range of 4000–500 cm^{-1} using a Cary 630 FTIR spectrometer (Agilent Technologies, Santa Clara, CA, USA). The spectra were collected from 128 scans at a resolution of 4 cm^{-1} for each sample.

Preparation of SWT-C reinforced paper sheets

A schematic diagram of the pulp pretreatment and paper sheet fabrication is shown in Fig. 1. Briefly, pulp/SWT-C dispersion and refining process for SW and HW was performed with the standard of TAPPI T200 sp-96 using a laboratory Valley beater to a freeness value of 350 mL CSF (Canadian Standard Freeness) (Mashkour et al. 2015). First, a SWT-C solution was prepared by dissolving 7 wt% of NaOH and 12 wt% of urea in distilled water at below 3°C. The resulting SWT-C solution was added to SW and HW suspensions, which were dispersed in distilled water at a content of 2 wt% following the ratios listed in Table 1. The paper sheets were controlled to have basis weights of 60 and 120 g/m^2. The prepared solution was dried by vacuum filtration through a Whatman filter No. 42 to form a wet sheet. To prepare the dry paper sheets, the wet sheets were first pressed at 30 bar for 5 min at room temperature, followed by hot pressing at 80°C and 25 bar for 10 min.

Twenty-eight different types of paper sheets were prepared in this study. The sheets were classified based on three variables: the type of pulp used (SW or HW), the basis weight (60 or 120 g/m²), and the concentration of SWT-C added (0, 1, 3, 9, 15, 20, 25, and 33.3 wt% based on the weight of SW or HW). To ensure clarity and consistency, each sample was named using the following format: [PulpType][BasisWeight]_[SWT-C concentration]%. For instance, a sheet made from SW pulp with no SWT-C and a basis weight of 120 g/m² is labeled as SW120_0%, while a paper sheet made from HW pulp with a basis weight of 60 g/m² and 1 wt% SWT-C is referred to as HW60_1%.

Table 1
Composition of paper sheets.

Pulp Type	Basis Weight (g/m^2)	Addition Ratio (w/w of SWT-C, %)
Control	60, 120	-
Softwood		1, 3, 9, 15, 20, 25, 33.3
Hardwood		

[1)] 'Control' refers to paper samples made from softwood and hardwood without the addition of SWT-C.

Structural, physical, and chemical properties of SWT-C reinforced paper sheets

Morphological properties were evaluated using a field-emission scanning electron microscope (FE-SEM, Apreo 2 S HiVac, Thermo Fisher Scientific, Waltham, MA, USA) at 250× magnification and an accelerating voltage of 5 kV. Image J software (National Institutes of Health, Bethesda, MD, USA) was employed to analyze the pore size of sample based on a SEM image scale bar of 300 μm.

The specific surface area and pore size distribution of the paper sheets were determined using Brunauer–Emmett–Teller (BET) analysis (Autosorb IQ; Quantachrome Instrument Co., Boynton Beach, FL, USA) by nitrogen gas adsorption and desorption at 77 K. Prior to the analysis, the samples were degassed under vacuum at 100°C to remove any physically adsorbed species.

The chemical structures of the paper sheet surface were evaluated using a Cary 630 FTIR spectrometer (Agilent Technologies, Santa Clara, CA, USA) for the measurement. Spectra were recorded across a wavenumber range of 650–4000 cm^{-1} with a resolution of 4 cm^{-1}.

X-ray diffraction (XRD) measurements were conducted using an X-ray diffractometer (D8-Advance, Bruker, Karlsruhe, Germany) operated at 40 kV and 40 mA. The diffraction patterns were recorded over a range from 5° to 60° with 2θ at 0.2 sec/step. MATLAB (MathWorks, Natick, MA, USA) was utilized to visualize the XRD patterns, and the crystallinity index was computed according to Segal's method (Segal et at. 1959) using the Eq. (1).

Mechanical and barrier properties of SWT-C reinforced paper sheets

The tensile strength of paper sheets was measured using a texture analyzer (TXA™ Standard Texture Analyzer, YEONJIN S-Tech Corporation, Yongin, Gyeonggi-do, South Korea) following ASTM D882 (ASTM, 2018). The test specimens were prepared with dimensions of 70 mm $\times$ 15 mm and the crosshead

speed was set to 1.00 mm/s. All tests were conducted under controlled conditions of 50 ± 2% relative humidity (RH) and 23 ± 1°C.

The Cobb60 values were measured at 23°C and 50% RH according to TAPPI standard T 441 om-13 (TAPPI, 2013). The Cobb value was calculated according to the following equation.

$$Cobb60 = \frac{W_2 - W_1}{A}$$

2

The percentage of water absorption was calculated as follows:

$$Water\ Absorption\ (\%) = \frac{W_2 - W_1}{W_1} \times 100$$

3

where W_1 represents the initial weight of the sample before water absorption (g), W_2 represents the final weight after water absorption (g), and A represents the area of the sample (m^2). For each sample, the average of three measurements was calculated.

Oil and grease resistance test was conducted following the TAPPI-T559 standard (TAPPI, 2012). Twelve vials of a mixture of castor oil, toluene, and n-heptane were prepared with a predetermined ratio, whereas kit 1 is the least aggressive oil and kit 12 is the most aggressive oil. A drop of the oil was placed onto the surface and wiped off after 15 sec. If darkening was observed, it was considered a failure; if not, a pass. The test was repeated to determine the highest kit number the paper could pass, which was recorded as its kit ranking.

Statistical analysis

ANOVA was performed with a significance level of $p < 0.05$, followed by Turkey's HSD test. Values are presented as mean ± standard deviation. Analyses were conducted using Python 3.9.13 (Python Software Foundation, Wilmington, DE, USA).

Results and discussion

Characteristics of SWT-C

Figure 2**(a)** shows the TEM images of SWT-C, revealing an entangled nanofibrillar network with a continuous and interconnected web-like morphology. This structure indicates that the subcritical water treatment facilitated the partial fibrillation of MCC, resulting in the formation of nanoscale fibrils. The average fibril diameter was measured to be 23.08 ± 5.37 nm, confirming effective defibrillation to the

nanoscale. This nanofibrillar structure may be suitable for forming percolated networks in both suspension and solid-state systems. Therefore, incorporation of SWT-C can enhance inter-fibril bonding and network formation, thereby improving the mechanical strength and barrier properties in cellulosic matrices.

Figure 2**(b)** presents the FTIR spectra of MCC and SWT-C. Both spectra exhibited characteristic cellulose bands. The broad absorption band at 3,600–3,200 cm^{-1} corresponds to O–H stretching vibrations, reflecting intramolecular and intermolecular hydrogen bonding within the cellulose structure. SWT-C exhibited a slightly higher intensity in this region compared to MCC, suggesting that the hydrogen-bonding cellulose framework remained intact with increased accessibility of surface hydroxy groups. The band near 2,900 cm^{-1} is attributed to C–H stretching vibrations, and the peak at 1,430 cm^{-1} corresponds to CH_2 bending, commonly considered an indicator of crystalline order in cellulose. SWT-C exhibited slightly higher intensity at 1,430 cm^{-1} relative to MCC, suggesting improved molecular organization and a reduction in amorphous regions. In the fingerprint region, strong absorptions between 1,200 and 1,000 cm^{-1} arise from C–O–C stretching of the β-(1→4) glycosidic linkages, characteristic of cellulose I. The band at approximately 897 cm^{-1}, often referred to as the amorphous band, is associated with C–H deformation coupled with C–O–C stretching at the anhydroglucose linkage. Furthermore, the absorption around 897 cm^{-1} showed no pronounced difference between the two samples, indicating that the β-(1→4) glycosidic linkages were largely retained after treatment. Overall, the retention of these characteristic bands and the absence of new peaks confirm that SWT primarily induced physical and microstructural rearrangement. This preserved integrity of cellulose, therefore, SWT-C may have advantages for acting as a paper additive, as it ensures predictable material behavior and minimizes the risk of undesirable side effects such as unintended oxidation during papermaking (Aziz et al. 2022). In addition, the increased accessibility of surface hydroxy groups indicates enhanced inter-fibril hydrogen bonding with pulp fibers, thereby promoting fiber–fiber interaction and network reinforcement in paper-based packaging materials.

Figure 2**(c)** shows the XRD patterns of MCC and SWT-C. Both samples exhibited the characteristic diffraction peaks of cellulose Iβ, with a broad reflection around $2\theta \approx 15–16°$ corresponding to the ($\bar{1}10$) and (110) planes and a strong, sharp peak at $2\theta \approx 22–23°$ assigned to the (200) plane. A minor peak observed near $2\theta \approx 34–35°$ was consistent with the (004) lattice plane of cellulose Iβ. These diffraction features confirm that the fundamental crystalline structure of cellulose Iβ was preserved after subcritical water treatment. The crystallinity of MCC was determined to be 74.53%, whereas SWT-C exhibited a higher value of 81.56%. This enhancement in crystallinity suggests that subcritical water treatment effectively removed amorphous domains of MCC, likely through partial hydrolysis of disordered cellulose regions, thereby enriching the crystalline fraction. This observation aligns with the crystallinity increase confirmed by FTIR analysis at 1,430 cm^{-1}. Such increased crystalline ordering may allow SWT-C to act as an effective reinforcing agent within paper fiber networks, as crystalline structured-cellulose typically exhibit higher stiffness and can facilitate load transfer (Altaner et al. 2014). In addition, the increased crystalline fraction of SWT-C may contribute to increased diffusion-path tortuosity when incorporated

into paper fiber networks, suggesting a potential benefit for barrier performance (Du et al. 2021; Fukuzumi et al. 2009; Wang et al. 2018).

Overall, MCC and SWT-C exhibited consistent fundamental structural features, confirming that the cellulose backbone was preserved after SWT. At the same time, SWT promoted nanoscale fibrillation and enhanced crystalline ordering without disrupting the essential chemical structure of cellulose. These findings suggest that SWT-C retains structural integrity while acquiring features favorable for reinforcement applications.

Appearance and surface texture of SWT-C reinforced paper sheets

Figure 3 exhibits the image of the paper sheets, enabling visual comparison of transparency and surface textures. As a result, as the concentration of SWT-C increased, transparency improved and the surface became smoother across all pulp types, including SW120, HW60, and HW120 (Table 2). In detail, the SW60_1% samples exhibited a white, opaque appearance with individual fibers partially visible to the naked eye (Fig. 3**(a)**). Also, its surface felt rough with a distinct fibrous texture. In contrast, the SW60_33.3% sample showed significantly increased transparency and a noticeably smoother surface, with a diminished fibrous texture (Fig. 3**(c)**). The SW60_9% samples displayed intermediate characteristics, retaining a whitish tone with partial translucency (Fig. 3**(b)**). These observations suggest that the addition of SWT-C induces structural modifications within the pulp matrix and facilitates new interactions between fibers. The present results indicate that the progressive increase in transparency and surface smoothness with higher SWT-C content further enhances the suitability of these materials for packaging applications (Spence 2016).

Table 2
Visual and texture characteristics of paper sheets as a function of SWT-C ratios.

SWT-C Concentration (%)	Visual Appearance	Surface Texture
1	Whitish, Fibrous	Rough and fibrous
9	Semi-transparent	Intermediate feel between fibrous and smooth
33.3	Transparent	Smooth

Morphology analysis of SWT-C reinforced paper sheets

SEM analysis was performed to investigate the effect of SWT-C on paper sheet morphology (Fig. 4). Figure 4**(a)** and **(d)** present the SEM images of SW and HW base papers without the addition of SWT-C, respectively. The surface exhibits an uneven and porous structure, which may lead to negative effects to the mechanical strength and barrier properties when applied as packaging materials. From Fig. 4**(a)** to **(c)** and Fig. 4**(d)** to **(f)**, while the amounts of SWT-C increased, the pores on the surface are progressively filled, resulting in a smoother and more compact surface. A noticeable reduction in surface porosity is

observed in the 9% of SWT-C added to the sheets (Fig. 4**(b)** and **(e)**) compared to sheets without SWT-C. As the SWT-C content further increased, the surface morphology became progressively more uniform, which is the most apparent in the samples containing the highest SWT-C content in this study (Fig. 4**(c)** and **(f)**). This morphological change can be attributed to the interaction between pulp fibers and SWT-C, where SWT-C particles fill the voids within the pulp network, contributing to pore closure and surface densification during blending.

Pore size distribution of SWT-C reinforced paper sheets

To evaluate the effects of SWT-C addition, DFT-based cumulative pore volume analysis and BET analysis were performed to assess changes in surface area and pore structure. The nitrogen adsorption-desorption isotherms for the paper sheets are presented in Fig. 5 and the BET surface areas and cumulative pore volumes of the different samples were determined from the N_2 adsorption isotherm data at 77 K, as shown in Table 3.

According to the IUPAC classification, most isotherms correspond to type IV with H3 hysteresis loops, indicating the presence of mesoporous structures formed by slit-like pores within the fiber network. However, 33.3% addition of SWT-C samples showed no hysteresis loop in all cases for both paper sheets (Fig. 5), implying a transition to a nonporous or microporous structure due to the densification of the fiber matrix (Thommes et al. 2015). This tendency is clearly reflected in the quantitative BET and pore volume data. As the SWT-C content increased, both BET surface area and cumulative pore volume consistently decreased. For instance, the SW120 group showed the most pronounced reduction, with the surface area dropping from 285.4 m^2/g at SW120_1% to 20.32 m^2/g at SW120_33.3%, and pore volume from 0.9546 cm^3/g to 0.04253 cm^3/g, representing 92.9% and 95.5% reductions, respectively. This is attributed to the incorporation of SWT-C into the fiber network, where the additive fills inter-fiber voids and suppresses mesopore formation, leading to reduced pore accessibility. These interpretations are further supported by the SEM images shown in Fig. 4, which show a gradual reduction in surface porosity and a more compact fiber arrangement with increasing SWT-C content. This morphological transition is consistent with the measured decreases in surface area and pore volume, confirming the structural densification induced by SWT-C incorporation.

Table 3
BET surface and DFT method cumulative pore volume of the paper sheets determined from the N_2 adsorption isotherm.

Sample			**BET specific surface area (m^2/g)**	**Pore Volume (cm^3/g)**
Pulp	Basis Weight (g/m^2)	Ratio (%)		
SW	60	1	215.5	0.6283
		9	265.1	0.9041
		33.3	62.41	0.0879
	120	1	285.4	0.9546
		9	200.7	0.6960
		33.3	20.32	0.0425
HW	60	1	211.6	0.2227
		9	184.9	0.3271
		33.3	147.7	0.1828
	120	1	91.18	0.1850
		9	64.48	0.0819
		33.3	52.65	0.0664

Crystallinity of SWT-C reinforced paper sheets

Figure 6 shows the XRD patterns of paper sheets with different SWT-C contents, and the corresponding crystallinity values are summarized in Table 4. All samples exhibited the characteristic diffraction peaks of cellulose I at 16° and 22°, indicating that the fundamental crystalline structure of cellulose was appeared after SWT-C incorporation (Montoya-Escobar et al. 2022). The crystallinity values showed minor variations with increasing SWT-C content. In the SW samples, the crystallinity slightly decreased at SW60_1% (65.3 ± 1.35%) and then increased at higher loadings of SWT-C, 67.9 ± 3.95% and 68.5 ± 2.97% for SW60_9% and SW60_33.3%, respectively. Similarly, the HW samples exhibited small fluctuations without a clear monotonic trend. Notably, the differences in crystallinity between the control and SWT-C-added samples were not statistically significant ($p > 0.05$). These results suggest that SWT-C incorporation does not substantially alter the overall crystalline structure of paper sheets.

Table 4
Crystallinity (%) of SWT-C–reinforced paper sheets prepared from (a) SW60 and (b) HW60 with SWT-C contents of 0%, 1%, 9%, and 33.3%.

Sample		Crystallinity (%)
Pulp	Ratio (%)	
SW	0	67.4 ± 0.92[a]
	1	65.3 ± 1.35[a]
	9	67.9 ± 3.95[a]
	33.3	68.5 ± 2.97[a]
HW	0	66.1 ± 1.01[a]
	1	66.6 ± 0.35[a]
	9	66.1 ± 1.15[a]
	33.3	67.4 ± 1.40[a]

[1)] Data are mean ± standard deviation ($n = 3$).

[2)] Significance levels, with the control group are indicated as $p > 0.05$.

Chemical structure of SWT-C reinforced paper sheets

Figure 7 presents the FTIR spectra of **(a)** SW60 and **(b)** HW60 paper sheets prepared with addition of SWT-C ratios for 9%, and 33.3%. The broad absorption band between 3,200 and 3,500 cm^{-1} corresponds to the stretching vibration of O–H groups in cellulose. With increasing SWT-C content, this band becomes broader, indicating stronger hydrogen bonding interactions within the cellulose matrix and greater heterogeneity in hydrogen bonding (Lee et al. 2015; Agarwal et al. 2011; Oh et al. 2005). Simultaneously, the overall reduction in O–H stretching band intensity with increasing SWT-C content indicates a decrease in free hydroxy groups on the fiber matrix. As a result, the capacity for moisture interaction is decreased, which may lead to enhanced water resistance (Olsson and Salmén 2004). In addition, the peak near 1,620 cm^{-1} is attributed to O–H bending vibrations, which specifically reflect changes in hydrogen-bonding strength within the cellulose structures (Athokpam et al. 2017). The increased absorbance observed in both SW_33.3% and HW_33.3% samples suggest the formation of stronger hydrogen bonds, as the intensities of these bands are known to correlate with hydrogen-bonding strength (Athokpam et al. 2017). The peaks at 1,430 cm^{-1} (CH_2 bending) and 898 cm^{-1} (β-1,4-glycosidic linkages, C-O-C stretching) were related to cellulose molecular structure order based on the absorbance ratio (A_{1430}/A_{898}) where a higher value suggests an increase in ordered cellulose domains

(Camarena-Bononad et al. 2024). The absorbance ratio increased from approximately 0.51 in SW_0% and HW_0% to 0.93 in SW60_33.3% and 1.07 in HW60_33.3%, indicating that SWT-C incorporation can enhance molecular orders in paper sheets and may contribute to improved mechanical strength and barrier performance. Considering the XRD results, this increase is more likely associated with enhanced surface-level ordering and inter-fiber hydrogen bonding rather than a substantial increase in bulk crystallinity. The FTIR results therefore suggest localized structural rearrangements and strengthened cellulose interactions within the fiber network, rather than a pronounced transformation of the crystalline phase.

The tensile strength of SWT-C reinforced paper sheets

The tensile strength of all SWT-C reinforced paper sheets tended to increase as the SWT-C content increased (Fig. 8). As a result, all paper sheets followed the same three-stage pattern of increase, decrease, and subsequent increase. As shown in Fig. 8, the tensile strength of the SWT-C reinforced paper sheets gradually increased with increasing SWT-C ratio up to 9%, a slight decrease was observed at 15% and followed by a subsequent increase with further addition up to 33.3%. SWT-C is a nano-sized material with a high aspect ratio which can enhance hydrogen bonding between cellulose fibers, thereby increasing the tensile strength of the SWT-C reinforced paper sheet at the first stage. However, tensile strength decreased due to the formation of voids and agglomerates of SWT-C at second stage similar with previous studies using nanocellulose (Aigaje et al. 2023). These defects originated from the repulsive interactions between densely packed SWT-C particles. As a result, efficient stress transfer across the matrix-filler interface was hindered, leading to reduced tensile strength (Aigaje et al. 2023). However, beyond a certain concentration, the reinforcing effects of hydrogen bonding and fiber interactions become dominant over repulsion, leading to a recovery and further increase in strength. For example, in the SW120 group, the strength increased to 21.86 MPa at 9% SWT-C, dropped to 17.87 MPa at 15%, and then rose again to 31.28 MPa at 33.3%. Among the all samples, the highest tensile strength was observed for HW120_33.3%, at 35.91 MPa. These numerical results are consistent with the proposed mechanism and clearly demonstrate the influence of SWT-C concentration on mechanical performance.

Moisture barrier properties of SWT-C reinforced paper sheets

The Cobb value represents the amount of water absorbed by paper over a given period and is inversely related to the water resistance of the material (Jin et al. 2021). As shown in Fig. 9, the Cobb60 values gradually decreased with increasing SWT-C content across all types of SWT-C reinforced paper sheet. This trend indicates that the addition of SWT-C contributes to reducing the water absorbency of the SWT-C reinforced paper sheet. This result suggests that the SWT-C particles partially filled the pores within the pulp network, thereby limiting the pathway for water penetration. In addition, increased hydrogen bonding between the SWT-C and pulp fibers strengthened the intra-interactions in the fiber network,

which provided a complementary mechanism for reducing water uptake. These trends are consistent with our previous observations from FTIR and tensile strength measurements. The results suggest that densification of the fiber structure and enhanced inter-fiber bonding play a central role in improving both mechanical strength and water resistance. In detail, in the SW60 group, the Cobb60 value decreased from 6.73 × 10¹ g/m² at 1% SWT-C to 1.37 × 10¹ g/m² at 33.3% SWT-C. Likewise, in the HW120 samples, the relative water absorption steadily declined from 15.07 × 10¹ g/m² at 1% SWT-C to 11.98 × 10¹ g/m² at 3%, 6.54 × 10¹ g/m² at 9%, 3.83 × 10¹ g/m² at 15%, and reached a minimum of 1.96 × 10¹ g/m² at 33.3%. In summary, the addition of SWT-C significantly improves the water resistance of paper by decreasing porosity and strengthening fiber interactions, as evidenced by the consistent reduction in both absolute Cobb values and normalized water absorption ratios.

Oil and grease resistance of SWT-C reinforced paper sheet

Figure 10 shows the oil and grease resistance results of paper sheets prepared in this study. As a result, as SWT-C content increased, the oil and grease resistance increased. The improved oil and grease resistance with increasing SWT-C content can be attributed to its ability to fill the existing pores in the pulp matrix, leading to a denser structure with smaller and fewer pores. The reduced pore size, lower pore density, and increased tortuosity of the diffusion pathway collectively hinder penetration, thereby enhancing the oil and grease resistance (Zhang and Youngblood 2023). Beyond the reduction in porosity, the enhanced oil and grease resistance of the SWT-C reinforced sheets arises from several interconnected structural and chemical effects introduced by SWT-C. First, the nanoscale fibrillar morphology of SWT-C creates a highly entangled network within the pulp matrix, forming a dense percolation structure that reduces the mobility of low-molecular-weight oils. This nanofibrillar network increases the tortuosity of the diffusion pathway far more effectively than pore-size reduction alone (Fig. 2a). Second, FTIR results indicate strengthened hydrogen bonding and a decrease in free hydroxy groups, which lowers the surface polarity of the paper sheet. This partial reduction in surface hydrophilicity can reduce the wettability of non-polar oils, thereby suppressing their spreading and penetration (Fig. 7). Third, the incorporation of SWT-C leads to closer packing of fibers and increased inter-fiber cohesion, forming a mechanically stiff and continuous barrier layer. Such cohesive fiber–filler junctions reduce inter-fiber capillary channels that oils typically exploit for permeation. Finally, the higher molecular ordering implied by the increased A_{1430}/A_{898} ratio suggests improved micro-scale structural alignment, which further reduces free volume and limits oil uptake. In detail, the SW120_33.3% and HW120_33.3% did not show any spots on the surface, even with kit number 12, whereas the SW120_1% and HW120_1% failed at kit number 1, as expected. The SW120_20% and HW120_20% showed no visible spots up to kit number 9, but staining appeared at kit number 10 (Table 5). The observation of high oil resistance even at 20% SWT-C content suggests that a loading of approximately 20% is sufficient to achieve effective oil barrier performance. Images of the oils used in the experiment are provided in the Supporting Information. Overall, these effects explain why the sheets containing 20% and 33.3% SWT-C exhibit high resistance even to aggressive oils up to kit level 12.

Table 5
Grease resistance testing of SWT-C reinforced paper sheet.

Sample		Kit level
Pulp	Ratio (%)	
SW	1	N.D*
	20	9
	33.3	12
HW	1	N.D*
	20	9
	33.3	12
*N.D. indicated 'Not determined'		

Conclusion

In this study, a paper-based packaging system incorporating SWT-C was developed, and improvements in mechanical strength and barrier properties were observed. The paper containing 33.3% of SWT-C exhibited enhanced transparency and surface smoothness compared to the unmodified paper. This result is attributed to a significant reduction in pore volume and specific surface area, as supported by SEM and BET analyses. The tensile strength followed a concentration-dependent trend, reaching the highest value of 35.91 MPa in the HW120_33.3% sample. XRD analysis showed no significant differences in crystallinity among the samples, regardless of SWT-C addition. This indicates that the observed improvements in mechanical strength and barrier properties were not directly associated with changes in crystallinity. Instead, the enhancement is primarily attributed to structural densification of the fiber network and strengthened inter-fiber interactions induced by SWT-C incorporation. Consistent with this interpretation, FTIR spectra showed increased intensity of hydroxy-related bands, indicating enhanced hydrogen bonding within the paper matrix. In terms of barrier performance, the Cobb60 value decreased substantially from approximately 232–368% absorbance at 1% of SWT-C to under 50% at 33.3% of SWT-C, while oil resistance was stably maintained up to kit level 12 in the 33.3% of SWT-C sample. These results suggest that SWT-C contributes to void filling and fiber network densification through hydrogen bonding, which leads to concurrent improvements in mechanical strength and barrier properties. Among the tested formulations, paper sheets containing 33.3% of SWT-C exhibited the most pronounced performance enhancement in both SW and HW systems. This reinforcement level supports the potential of SWT-C–reinforced paper as an eco-friendly packaging material with improved moisture and oil resistance, as well as suitability for high-strength packaging applications.

Declarations

Authorship contribution statement

Suhyeon Nam: Methodology, Validation, Formal analysis, Investigation, Resources, Data Curation, Writing – Original Draft, Writing – Review & Editing, Visualization

Jiho Lim: Methodology, Validation, Formal analysis, Investigation, Resources, Data Curation, Writing – Original Draft, Writing – Review & Editing, Visualization

Soohyun Kim: Methodology, Validation, Investigation, Data Curation, Writing – Original Draft, Writing – Review & Editing, Visualization

Ji Hun Park: Writing – Review & Editing

Hansol Doh: Conceptualization, Methodology, Formal analysis, Investigation, Writing – Original Draft, Writing – Review & Editing, Visualization, Supervision, Project administration, Funding acquisition

Declaration of Competing Interest

The authors declare that they have no known competing financial interests or personal relationships that could have appeared to influence the work reported in this paper.

Acknowledgement / Funding sources

This work was supported by the National Research Foundation of Korea (NRF) grant funded by the Korea government (MSIT) (No. RS-2022-00166093 and No. RS-2023-00248098).

Data availability

Data will be made available on request.

References

1. Abdul Rashid ES, Julkapli NM, Yehye WA (2018) Nanocellulose reinforced as green agent in polymer matrix composites applications. *Polym Adv Technol* 29(10):2564–2581. https://doi.org/10.1002/pat.4264
2. Adschiri T, Hirose S, Malaluan R, Arai K (1993) Noncatalytic conversion of cellulose in supercritical and subcritical water. *J Chem Eng Jpn* 26(6):676–680. https://doi.org/10.1252/jcej.26.676
3. Agarwal V, Huber GW, Conner WC Jr, Auerbach SM (2011) Simulating infrared spectra and hydrogen bonding in cellulose Iβ at elevated temperatures. *J Chem Phys* 135(13):134506. https://doi.org/10.1063/1.3646306
4. Aigaje E, Riofrio A, Baykara H (2023) Processing, properties, modifications, and environmental impact of nanocellulose/biopolymer composites: A review. *Polymers* 15(5):1219. https://doi.org/10.3390/polym15051219

5. Alava M, Niskanen K (2006) The physics of paper. *Rep Prog Phys* 69(3):669–723. https://doi.org/10.1088/0034-4885/69/3/R03
6. Altaner CM, Thomas LH, Fernandes AN, Jarvis MC (2014) How cellulose stretches: synergism between covalent and hydrogen bonding. *Biomacromolecules* 15(3):791–798. https://doi.org/10.1021/bm401616n
7. ASTM International (2018) ASTM D882-18: Standard test method for tensile properties of thin plastic sheeting. ASTM International. https://doi.org/10.1520/D0882-18
8. Aziz T, Farid A, Haq F et al (2022) A review on the modification of cellulose and its applications. *Polymers* 14(15):3206. https://doi.org/10.3390/polym14153206
9. Athokpam B, Ramesh SG, McKenzie RH (2017) Effect of hydrogen bonding on the infrared absorption intensity of OH stretch vibrations. *Chem Phys* 488–489:43–54. https://doi.org/10.1016/j.chemphys.2017.03.006
10. Barbash V, Yashchenko O, Gondovska A, Deykun I (2022) Preparation and characterization of nanocellulose obtained by TEMPO-mediated oxidation of organosolv pulp from reed stalks. *Appl Nanosci* 12(4):835–848. https://doi.org/10.1007/s13204-021-02061-1
11. Camarena-Bononad P, Freitas PAV, Chiralt A, Vargas M (2024) Subcritical water extraction for recovering cellulose fibres from Posidonia oceanica waste. *Carbohydr Polym Technol Appl* 8:100550. https://doi.org/10.1016/j.carpta.2024.100550
12. Ciolacu DE, Ciolacu F, Popa VI (2011) Amorphous cellulose – structure and characterization. *Cellul Chem Technol* 45(1):13–21
13. Deng Z, Jung J, Zhao Y (2017) Development, characterization, and validation of chitosan adsorbed cellulose nanofiber (CNF) films as water resistant and antibacterial food contact packaging. *LWT–Food Sci Technol* 83:132–140. https://doi.org/10.1016/j.lwt.2017.05.013
14. Doh H, Lee MH, Whiteside WS (2020) Physicochemical characteristics of cellulose nanocrystals isolated from seaweed biomass. *Food Hydrocoll 102:105542*.https://doi.org/10.1016/j.foodhyd.2019.105542
15. Du L, Yu H, Zhang B, Tang R, Zhang Y, Qi C, Wolcott MP, Yu Z, Wang J (2021) Transparent oxygen barrier nanocellulose composite films with a sandwich structure. *Carbohydr Polym* 268:118206. https://doi.org/10.1016/j.carbpol.2021.118206
16. Fukuzumi H, Saito T, Iwata T, Kumamoto Y, Isogai A (2009) Transparent and high gas barrier films of cellulose nanofibers prepared by TEMPO-mediated oxidation. *Biomacromolecules* 10(1):162–165. https://doi.org/10.1021/bm801065u
17. Furuheim KM, Axelson DE, Antonsen HW, Helle T (2004) Phase structural analyses of polyethylene extrusion coatings on high-density papers. II. Influence of paper surface properties on the polyethylene morphology. *J Appl Polym Sci 91(1):226–234.* https://doi.org/10.1002/app.13185
18. Guan M, An X, Liu H (2019) Cellulose nanofiber (CNF) as a versatile filler for the preparation of bamboo pulp based tissue paper handsheets. *Cellulose 26*(4):2613–2624. https://doi.org/10.1007/s10570-018-2212-6

19. Hubbe MA, Rojas OJ, Lucia LA, Sain M (2008) Cellulosic nanocomposites: A review. *BioResources 3*(3):929–980. https://doi.org/10.15376/biores.3.3.929-980
20. Jin K, Tang Y, Liu J, Wang J, Ye C (2021) Nanofibrillated cellulose as coating agent for food packaging paper. *Int J Biol Macromol 168:331–338.* https://doi.org/10.1016/j.ijbiomac.2020.12.066
21. Ko MJ, Nam HH, Chung MS (2020) Subcritical water extraction of bioactive compounds from *Orostachys japonicus* A. Berger (Crassulaceae). *Sci Rep 10:*10890. https://doi.org/10.1038/s41598-020-67508-2
22. Laleicke PF, Hubbe MA (2025) Outdoor wood finishing: A review on making wood resistant to moisture, ultraviolet light, and degradation. *BioResources 20*(3):7903–7940. https://doi.org/10.15376/biores.20.3.Laleicke
23. Lee CM, Kubicki JD, Fan B, Zhong L, Jarvis MC, Kim SH (2015) Hydrogen-bonding network and OH stretch vibration of cellulose: Comparison of computational modeling with polarized IR and SFG spectra. *J Phys Chem B 119*(49):15138–15149. https://doi.org/10.1021/acs.jpcb.5b08015
24. Lei W, Hou J, Fang C, Qin J, Zhou X, Li L (2024) High-efficiency modification of PET by the low addition of a self-assembled functional nanocellulose film prepared from waste paper. *Polym Compos 45*(6):3355–3366. https://doi.org/10.1002/pc.28648
25. Li A, Xu D, Luo L et al (2021) Overview of nanocellulose as additives in paper processing and paper products. *Nanotechnol Rev 10*(1):264–281. https://doi.org/10.1515/ntrev-2021-0023
26. Li B, Xu W, Kronlund D et al (2015) Cellulose nanocrystals prepared via formic acid hydrolysis followed by TEMPO-mediated oxidation. *Carbohydr Polym 133:*605–612. https://doi.org/10.1016/j.carbpol.2015.07.033
27. Lu Z, Zhang H, Liu L et al (2023) Study on cellulose nanofibers (CNF) distribution behaviors and their roles in improving paper property. *Ind Crops Prod 201:*116897. https://doi.org/10.1016/j.indcrop.2023.116897
28. Marzbani P, Azadfallah M, Yousefzadeh M, Tarmian A (2021) Effect of polyethylene wax/soy protein-based dispersion barrier coating on the physical, mechanical, and barrier characteristics of paperboards. *J Coat Technol Res 18*(1):247–257. https://doi.org/10.1007/s11998-020-00403-7
29. Mashkour M, Afra E, Resalati H, Mashkour M (2015) Moderate surface acetylation of nanofibrillated cellulose for the improvement of paper strength and barrier properties. *RSC Adv 5*(74):60352–60360. https://doi.org/10.1039/C5RA08161K
30. Mohomane SM, Motloung SV, Koao LF, Motaung TE (2022) Effects of acid hydrolysis on the extraction of cellulose nanocrystals (CNCs): A review. *Cellul Chem Technol 56*(7–8):691–703. https://doi.org/10.35812/CelluloseChemTechnol.2022.56.61
31. Montoya-Escobar N, Ospina-Acero D, Velásquez-Cock JA et al (2022) Use of Fourier series in X-ray diffraction (XRD) analysis and Fourier-transform infrared spectroscopy (FTIR) for estimation of crystallinity in cellulose from different sources. *Polymers 14*(23):5199. https://doi.org/10.3390/polym14235199

32. Novo LP, Bras J, García A, Belgacem N, Curvelo AAS (2015) Subcritical water: A method for green production of cellulose nanocrystals. *ACS Sustain Chem Eng 3*(11):2839–2846. https://doi.org/10.1021/acssuschemeng.5b00762
33. Oh SY, Yoo DI, Shin Y et al (2005) Crystalline structure analysis of cellulose treated with sodium hydroxide and carbon dioxide by means of X-ray diffraction and FTIR spectroscopy. *Carbohydr Res 340*(15):2376–2391. https://doi.org/10.1016/j.carres.2005.08.007
34. Oh Y, Park SY, Yook S, Kim J, Lee H (2022) A waterproof cellulose nanofibril sheet prepared by the deposition of an alkyl ketene dimer on a controlled porous structure. *Cellulose 29:*6645–6657. https://doi.org/10.1007/s10570-022-04701-8
35. Olsson A-M, Salmén L (2004) The association of water to cellulose and hemicellulose in paper examined by FTIR spectroscopy. *Carbohydr Res 339*(4):813–818. https://doi.org/10.1016/j.carres.2004.01.005
36. Osei-Bonsu R, Hoque M, McMichael PS, Foster EJ (2024) Subcritical water digestion of woody biomass: Extraction of cellulose nanomaterials under acid-lean condition. *Nanoscale Adv 6*(15):11140–11149. https://doi.org/10.1039/D4NA00108G
37. Perdoch W, Cao Z, Florczak P et al (2022) Influence of nanocellulose structure on paper reinforcement. *Molecules 27*(15):4696. https://doi.org/10.3390/molecules27154696
38. Potenza M, Bergamonti L, Lottici PP et al (2022) Green extraction of cellulose nanocrystals of polymorph II from *Cynara scolymus* L.: Challenge for a “zero waste” economy. *Crystals 12*(5):672. https://doi.org/10.3390/cryst12050672
39. Prakash B, Kumar A, Singh PP, Songachan LS (2020) Antimicrobial and antioxidant properties of phytochemicals: Current status and future perspective. In: Grumezescu AM, Holban AM (eds) *Functional and preservative properties of phytochemicals*. Academic Press, pp 1–45. https://doi.org/10.1016/B978-0-12-818593-3.00001-4
40. Rafeny NHB, Bahruji H, Abdullah R, Mahadi AH, Prasetyoko D (2023) Subcritical water hydrolysis of cotton fibers to nanocellulose for producing poly (vinyl alcohol)/cellulose biocomposite. *Starch-Stärke 75*(9–10):2300065. https://doi.org/10.1002/star.202300065
41. Spence C (2016) Multisensory packaging design: Color, shape, texture, sound, and smell. In: Delarue I (ed) *Integrating the packaging and product experience in food and beverages: A road-map to consumer satisfaction*. Woodhead Publishing, pp 1–22. https://doi.org/10.1016/B978-0-08-100356-5.00001-2
42. TAPPI (2022) *Grease resistance test for paper and paperboard (TAPPI T 559 cm-22).* Technical Association of the Pulp and Paper Industry.
43. Thommes M, Kaneko K, Neimark AV et al (2015) Physisorption of gases, with special reference to the evaluation of surface area and pore size distribution (IUPAC technical report). *Pure Appl Chem 87*(9–10):1051–1069. https://doi.org/10.1515/pac-2014-1117
44. Wang C, Shi J, He M et al (2018) High strength cellulose/ATT composite films with good oxygen barrier property for sustainable packaging applications. *Cellulose* 25(7):4145–4154.

https://doi.org/10.1007/s10570-018-1855-7

45. Wohlert M, Benselfelt T, Wågberg L, Berglund LA (2022) Cellulose and the role of hydrogen bonds: Not in charge of everything. *Cellulose 29*:1–23. https://doi.org/10.1007/s10570-021-04325-4

46. Zhang J, Youngblood JP (2023) Cellulose nanofibril (CNF)-coated PFAS-free, grease-resistant all-bio-based molded pulp containers for food packaging. *ACS Appl Polym Mater 5*(7):5696–5706. https://doi.org/10.1021/acsapm.3c00979

Figures

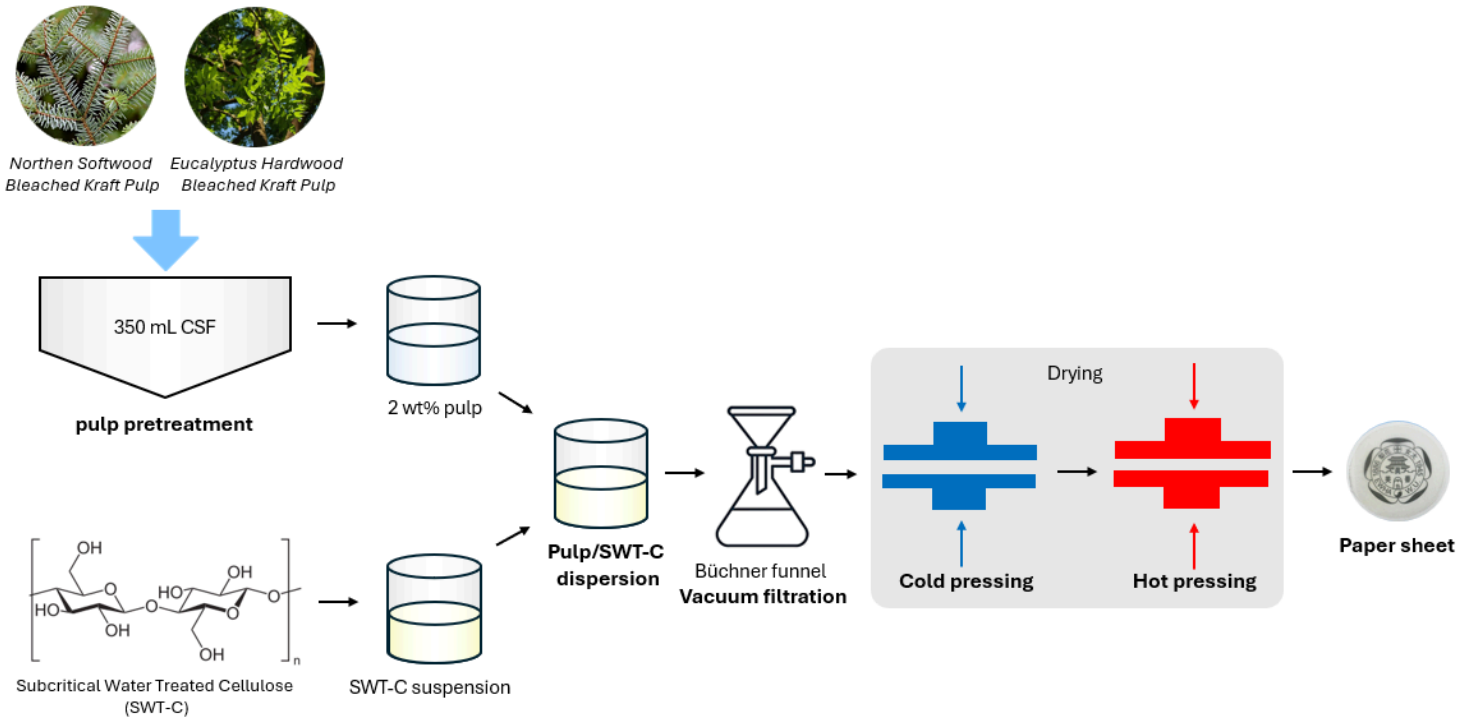


Figure 1

Scheme of SWT-C reinforced paper sheet formation.

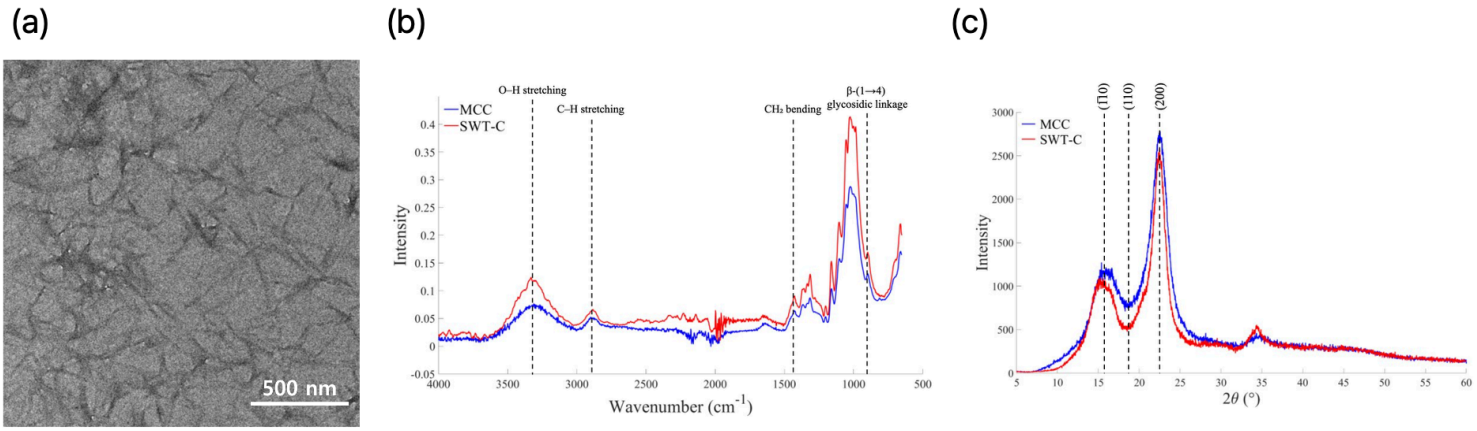


Figure 2

Structural, physical, and chemical properties of SWT-C. TEM images, (a); FTIR, (b); XRD, (c).

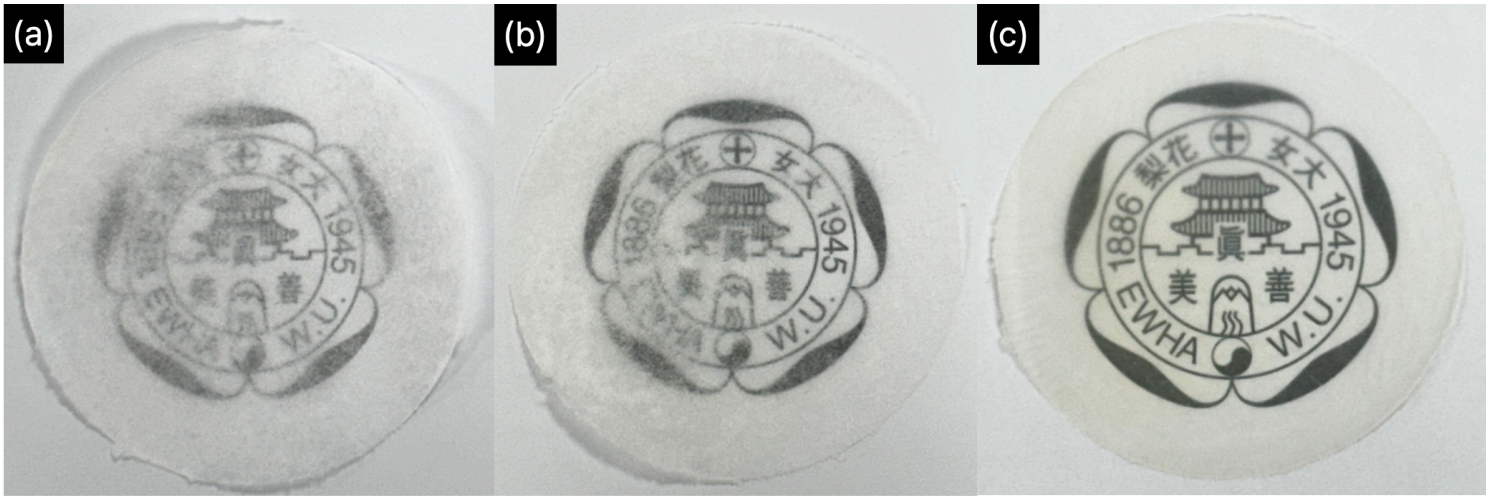


Figure 3

Visual comparison of SWT-C reinforced paper sheets prepared with different SWT-C ratios: (a) SW60_1%, (b) SW60_9%, and (c) SW60_33.3%.

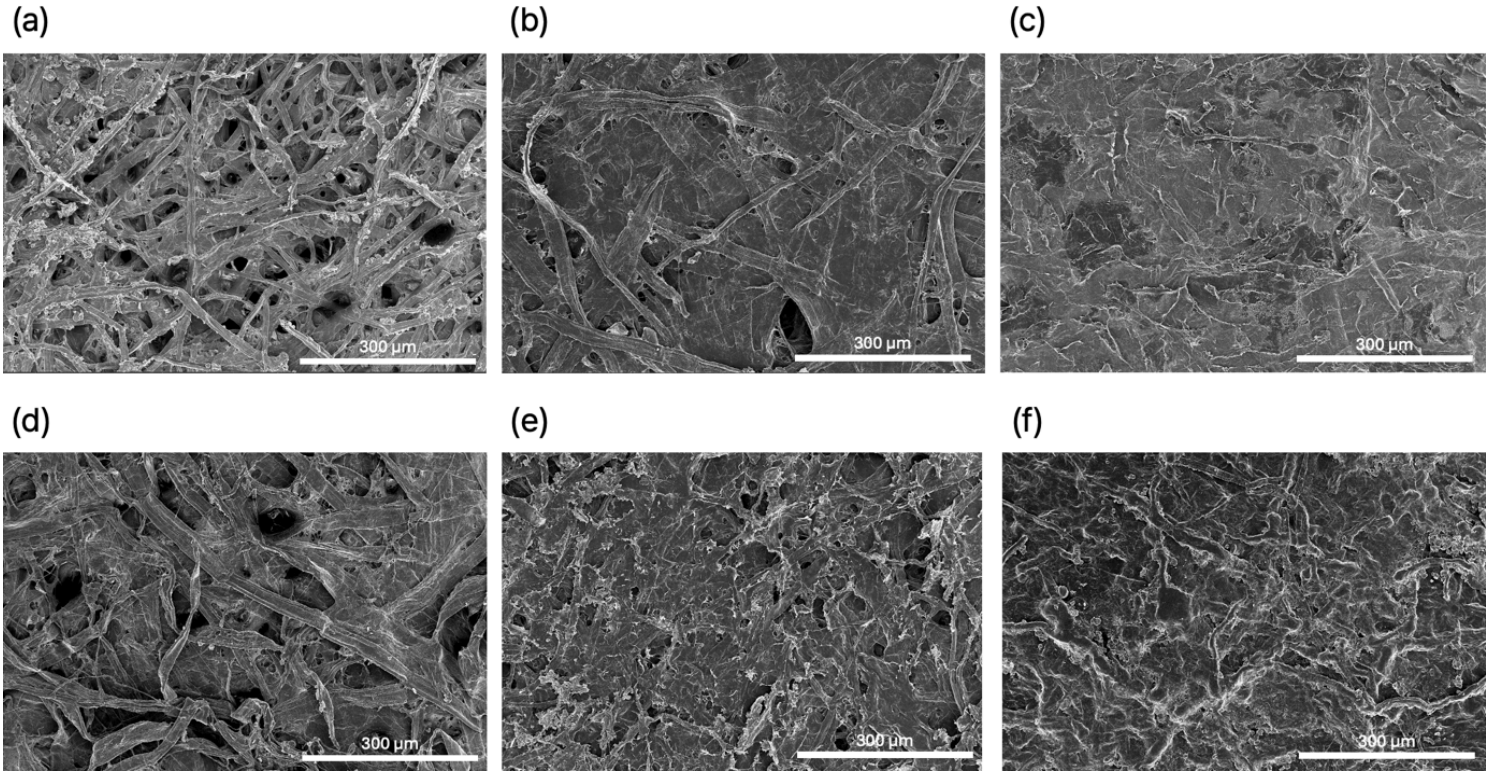


Figure 4

SEM images of SWT-C reinforced paper sheets prepared with different SWT-C ratios: (a) SW_0%, (b) SW_9%, (c) SW_33.3%, (d) HW_0%, (e) HW_9%, (f) HW_33.3%.

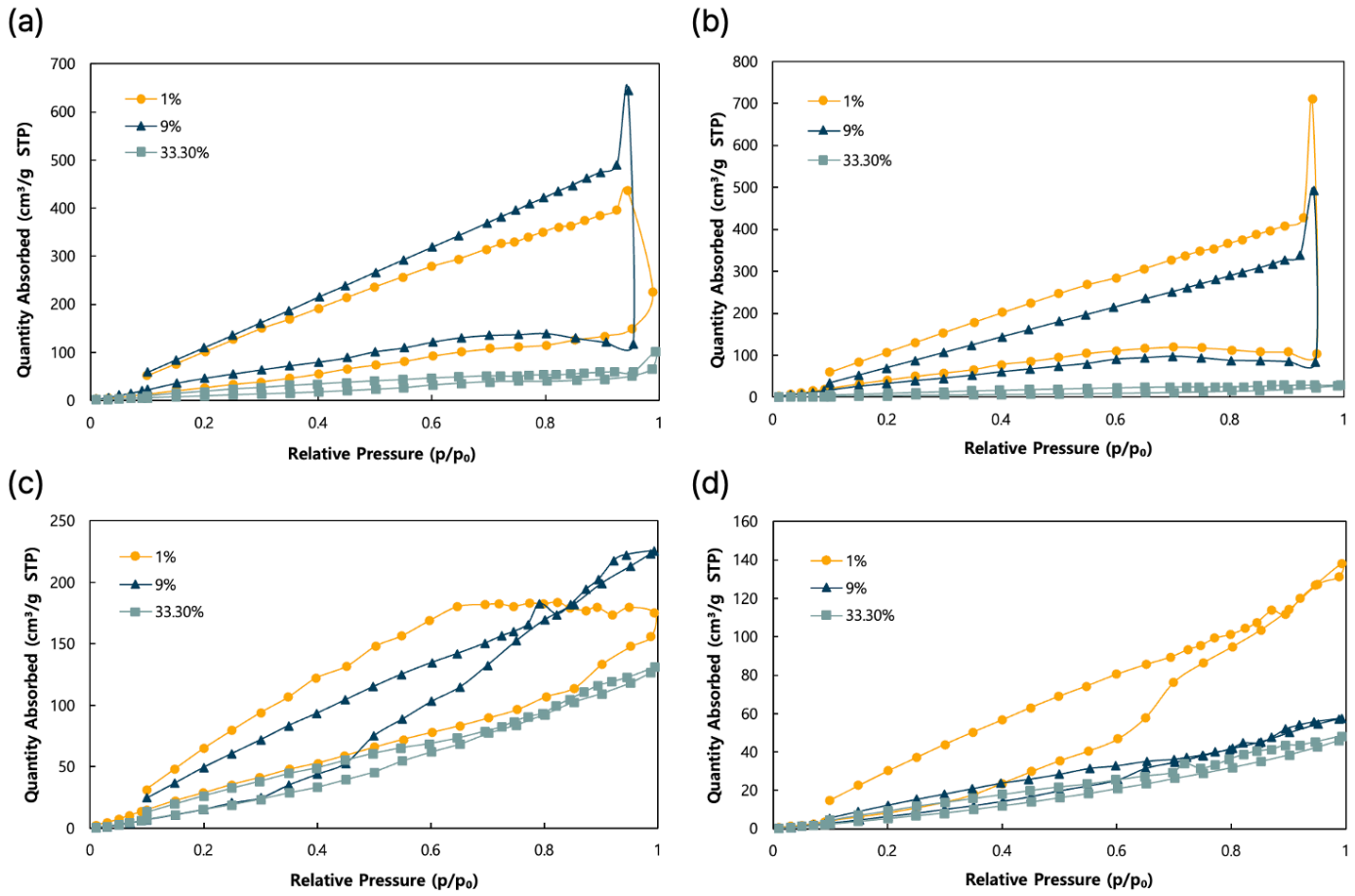


Figure 5

Nitrogen adsorption-desorption isotherms for the (a) SW60, (b) SW120, (c) HW60, (d) HW120 at 77 K.

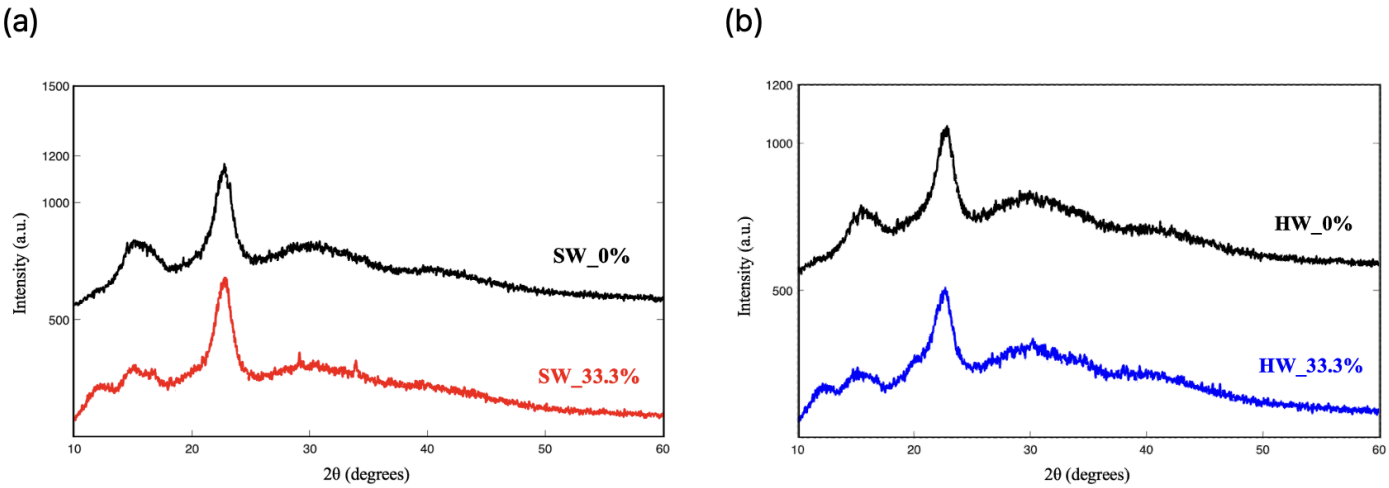


Figure 6

The X-ray diffraction patterns of SWT-C reinforced paper sheets: (a) SW60_0% and SW60_33.3%, and (b) HW60_0% and HW60_33.3%.

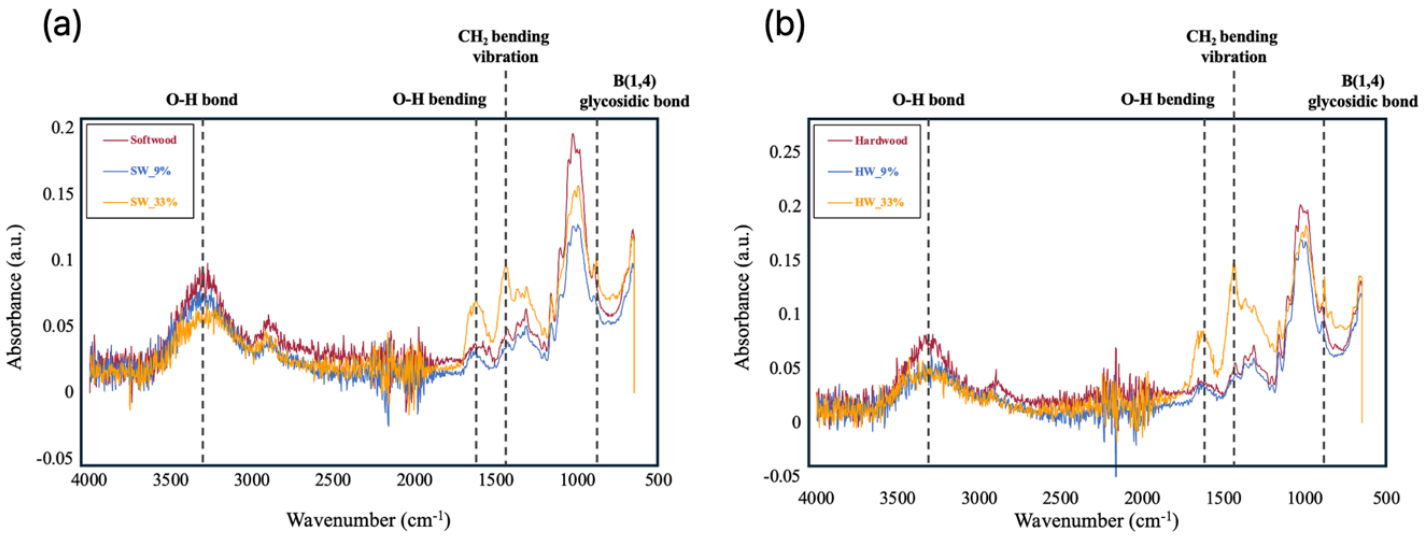


Figure 7

FTIR spectra of SWT-C–reinforced paper sheets prepared from (a) SW60 and (b) HW60 with SWT-C contents of 1%, 9%, and 33.3%.

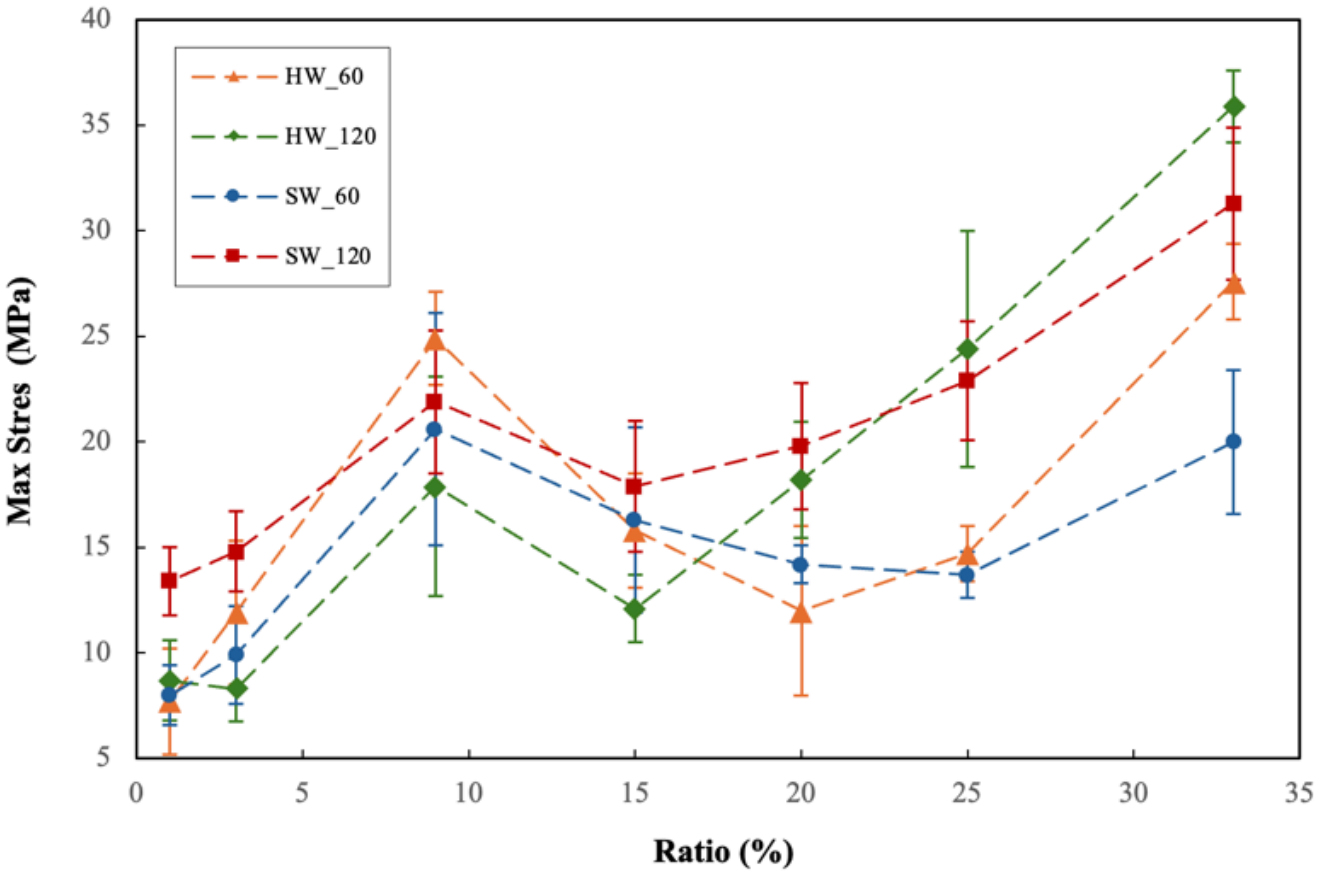


Figure 8

Max stress of SWT-C reinforced paper sheet at different SWT-C ratios (1–33.3%) using SW and HW pulp at two basis weights (60 and 120 g/m²).

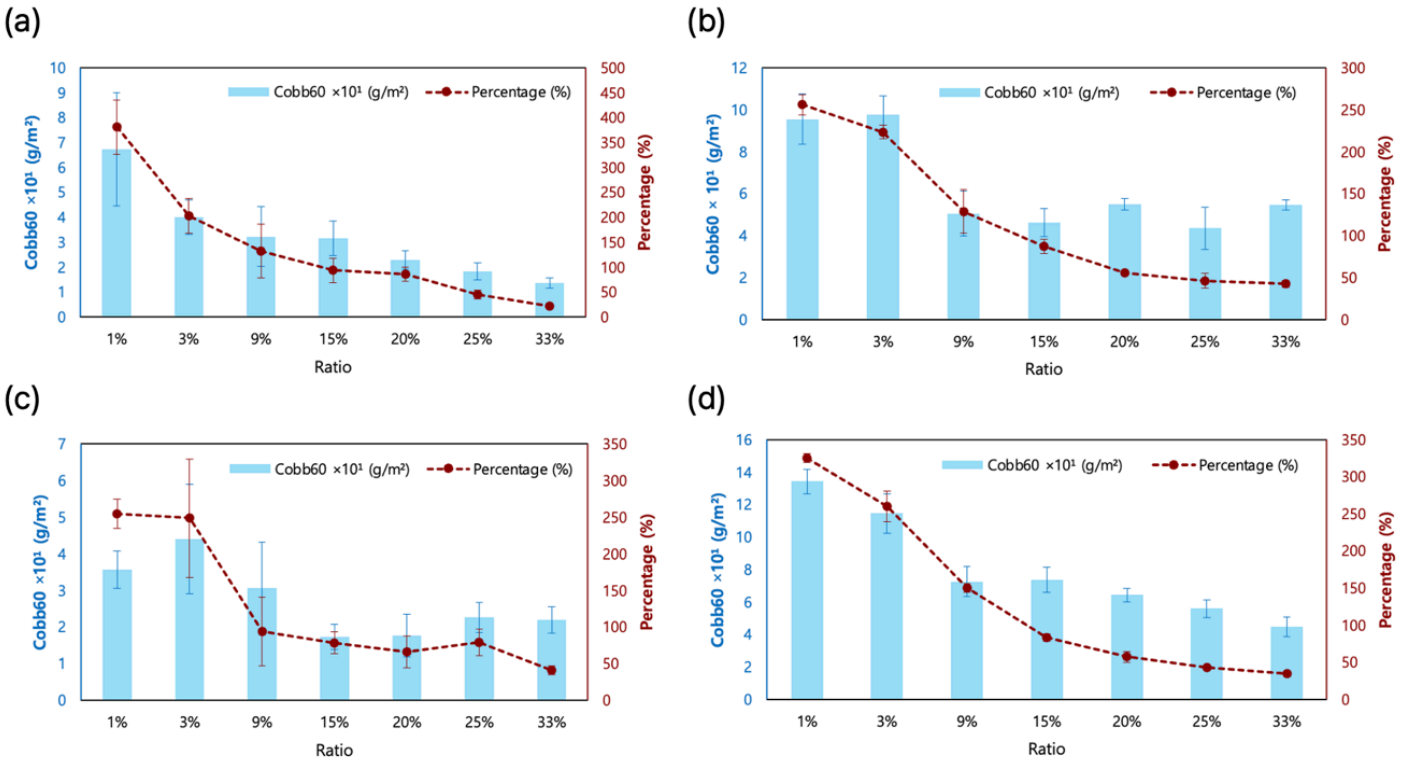


Figure 9

Cobb60 values and relative reduction (%) at different SWT-C ratio**:** (a) SW60, (b) SW120, (c) HW60, (d) HW120.

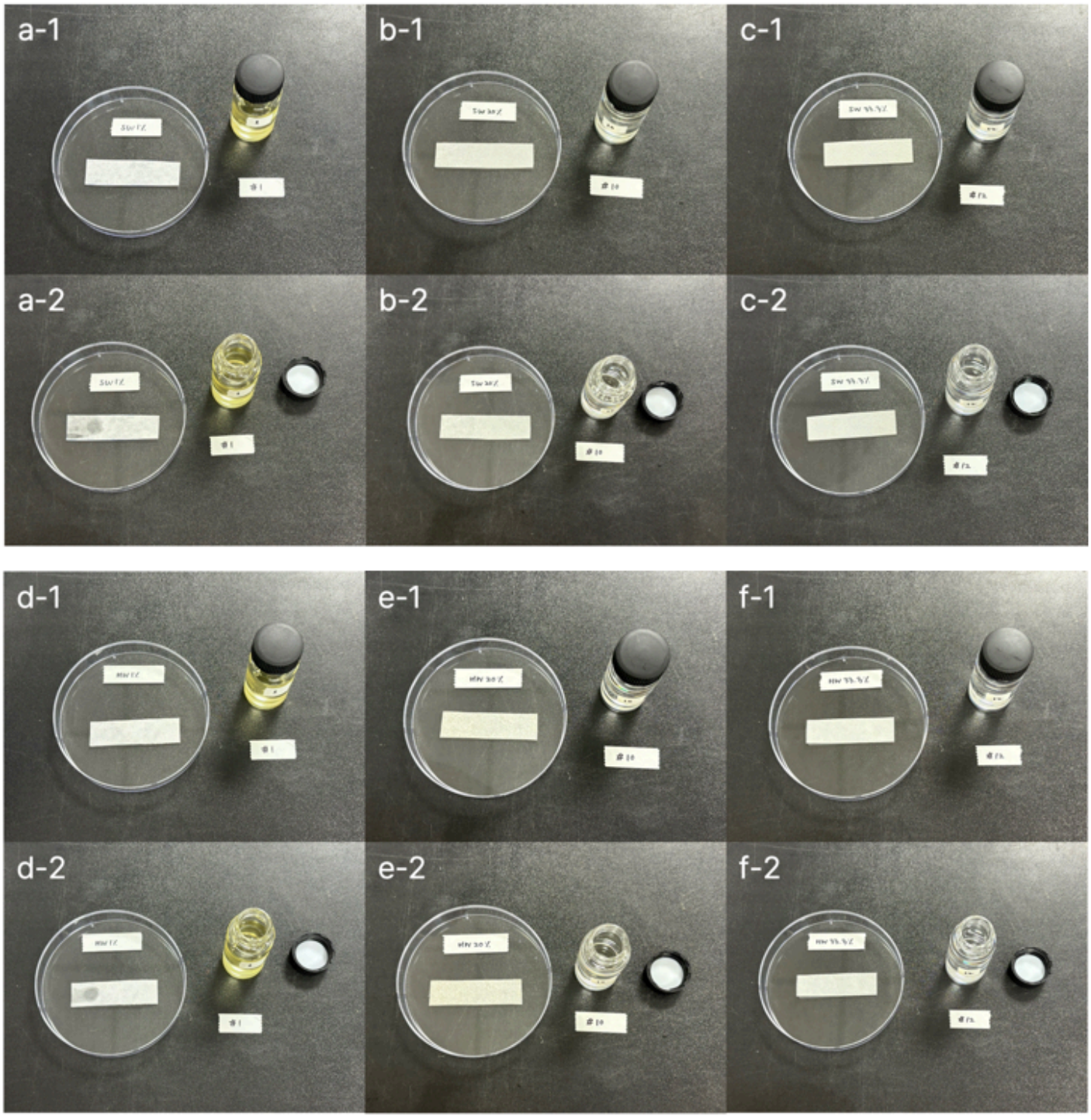


Figure 10

Grease resistance of SWT-C–reinforced paper sheets at different SWT-C contents (1%, 20%, 33.3%). Images show the surface appearance before and after exposure to each corresponding kit level: (a) SW120_1% at kit level 1, (b) SW120_20% at kit level 10, (c) SW120_33.3% at kit level 12, (d) HW120_1% at kit level 1, (e) HW120_20% at kit level 10, and (f) HW120_33.3% at kit level 12.